

Homoleptic Cerium(III) and Cerium(IV) Nitroxide Complexes: Significant Stabilization of the 4+ Oxidation State

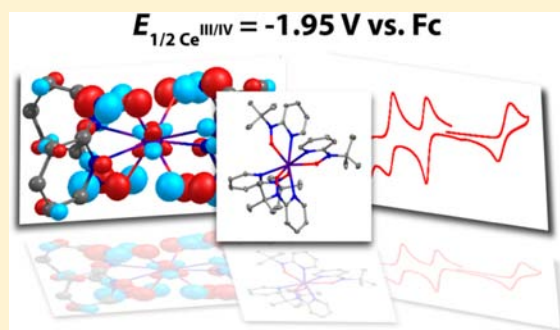
Justin A. Bogart,[†] Andrew J. Lewis,[†] Scott A. Medling,[‡] Nicholas A. Piro,[†] Patrick J. Carroll,[†] Corwin H. Booth,[‡] and Eric J. Schelter^{*,†}

[†]P. Roy and Diana T. Vagelos Laboratories, Department of Chemistry, University of Pennsylvania, Philadelphia, Pennsylvania 19104, United States

[‡]Chemical Sciences Division, Lawrence Berkeley National Laboratory, Berkeley, California 94720, United States

S Supporting Information

ABSTRACT: Electrochemical experiments performed on the complex $\text{Ce}^{\text{IV}}[2\text{-}(t\text{BuNO})\text{py}]_4$, where $[2\text{-}(t\text{BuNO})\text{py}]^- = N\text{-tert-butyl-}N\text{-2-pyridylnitroxide}$, indicate a 2.51 V stabilization of the 4+ oxidation state of Ce compared to $[\text{Bu}_4\text{N}]_2[\text{Ce}(\text{NO}_3)_6]$ in acetonitrile and a 2.95 V stabilization compared to the standard potential for the ion under aqueous conditions. Density functional theory calculations suggest that this preference for the higher oxidation state is a result of the tetrakis(nitroxide) ligand framework at the Ce cation, which allows for effective electron donation into, and partial covalent overlap with, vacant 4f orbitals with δ symmetry. The results speak to the behavior of CeO_2 and related solid solutions in oxygen uptake and transport applications, in particular an inherent local character of bonding that stabilizes the 4+ oxidation state. The results indicate a cerium(IV) complex that has been stabilized to an unprecedented degree through tuning of its ligand-field environment.



INTRODUCTION

Cerium oxides and their solid solutions are used extensively in heterogeneous catalysis for the water-gas shift reaction,^{1,2} in three-way catalytic converters,^{3,4} and as electrolyte materials in solid oxide fuel cells.^{5,6} Such materials are of broad intense interest for applications requiring the uptake and release of oxygen,⁷ including the mitigation of oxidative damage in vivo for the proposed treatment of ischemic stroke,⁸ Alzheimer's disease,⁹ and cancers.¹⁰ The reversibility of oxygen transport is understood to derive from localized electronic structure, where an electron is transferred to a nonbonding Ce 4f orbital concomitant with reorganization of the metal–oxide lattice.^{11–13} In all cases, materials performance is directly dependent on the thermodynamics of the redox change between the Ce^{III} and Ce^{IV} oxidation states.¹⁴ However, single-crystalline cubic CeO_2 , which provides the thermodynamic parentage for oxygen transport, exhibits a remarkable and peculiar resistance to reduction.^{15–17}

In this context, we became interested in model coordination compounds that emulate and elucidate the electronic structure and bonding in cerium oxides and related materials. The nonbonding character of the localized 4f electron in reduced cerium oxides led us to reason that such model compounds would accurately capture the structure and bonding inherent to the redox chemistry. Because of the interesting resistance of crystalline CeO_2 to reduction, our initial aims for this work were to develop discrete cerium coordination compounds in symmetric geometries and study their redox chemistry,

(in)stability in each redox form, and associated electronic structures. We expected that cerium complexes that structurally mimic CeO_2 would benefit from a similar stabilization of the 4+ oxidation state.

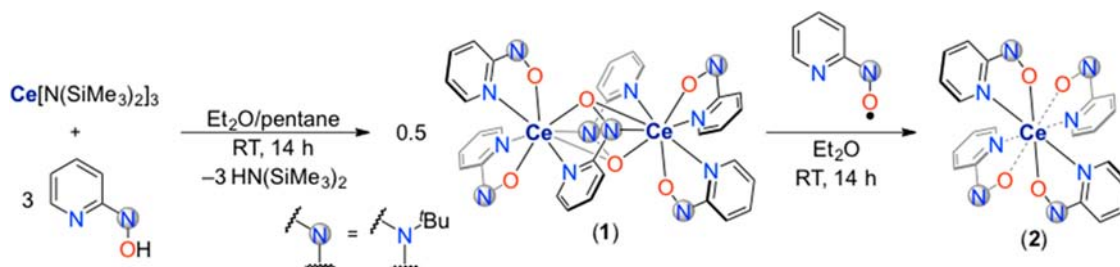
High-valent transition-metal complexes are stabilized by the coordination of electronegative elements such as oxygen¹⁸ or fluorine,¹⁹ bulky and electron-rich ligands,^{20–22} and crystal-field environments that favor low d-electron counts.²³ In contrast, the requirements for stabilizing high-oxidation-state molecular complexes of the lanthanides, in particular cerium(IV),^{24–27} are considerably less developed. Eller and Penneman concluded that oxygen-donor ligands stabilize cerium(IV) complexes because of the large electronegativity of oxygen.²⁸ Electrochemical studies performed on aqueous solutions of cerium in $\text{NaHCO}_3/\text{Na}_2\text{CO}_3$ buffers show a remarkable stabilization of the $\text{Ce}^{\text{III/IV}}$ couple by up to ~ 1.7 V.²⁹ Even neutral oxygen donors can strongly stabilize the Ce^{IV} cation; triphenylarsine oxide complexes of $\text{Ce}(\text{NO}_3)_3$ in an acetonitrile solution spontaneously oxidize in air.³⁰ Similarly, in $\text{Sm}^{\text{II/III}}$ -mediated reduction chemistry, the choice of the supporting ligand can have a profound effect on the redox potential and reactivity.^{31–34}

Because of their potential for redox activity and role as anionic oxygen-donor ligands, we hypothesized that four nitroxide ligands coordinated to a cerium cation could

Received: July 30, 2013

Published: September 11, 2013

Scheme 1. Syntheses of Complexes 1 and 2



coordinatively saturate and electronically stabilize the ion to act as effective surrogates for the eight-coordinate ligand field in CeO_2 . We report here that the homoleptic nitroxide complex $\text{Ce}^{\text{IV}}[2\text{-}(\text{tBuNO})\text{py}]_4$ (**2**) shows an unprecedented stabilization of the Ce^{IV} ion by the nitroxide framework, as judged by solution-phase electrochemistry and X-ray absorption spectroscopy (XAS) in the solid state. Density functional theory (DFT) calculations on **2** and its anion underscore stabilization of the Ce^{IV} oxidation state through enhanced electron donation provided by the partially covalent and symmetric ligand framework.

RESULTS AND DISCUSSION

Syntheses and Complex Characterization. In pursuit of a homoleptic cerium(IV) nitroxide complex, we first prepared a dimeric cerium(III) complex, $[\text{Ce}^{\text{III}}(\mu\text{-}2\text{-}(\text{tBuNO})\text{py})(2\text{-}(\text{tBuNO})\text{py})_2]_2$ (**1**). Layering a pentane solution of $\text{Ce}[\text{N}(\text{SiMe}_3)_2]_3$ upon an Et_2O solution of $2\text{-}(\text{tBuNOH})\text{py}$ ³⁵ led to the deposition of dark-red crystals of **1** in 66% yield (Scheme 1). Complex **1** is sparingly soluble in common organic solvents and rapidly oxidizes to a dark solid in the presence of oxygen. Although the poor solubility of complex **1** prevented its solution characterization by ^1H NMR spectroscopy, its composition was confirmed by elemental analysis and X-ray crystallography (Figure 1).

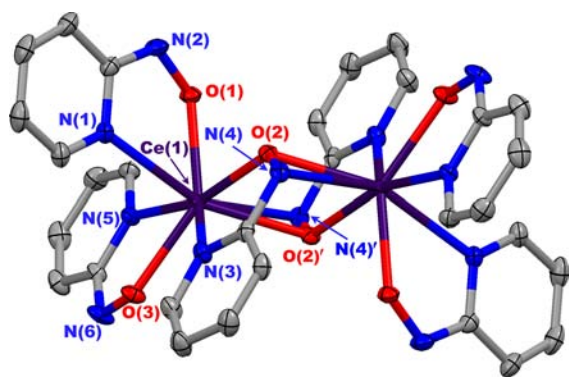


Figure 1. Thermal ellipsoid plot of **1** at 30% probability. Hydrogen atoms and *tert*-butyl groups are omitted for clarity. Selected bond distances (Å): Ce(1)–N(1) 2.596(2), Ce(1)–O(1) 2.306(2), Ce(1)–N(4) 2.687(2), Ce(1)–O(2) 2.427(2), N(2)–O(1) 1.370(3), N(4)–O(2) 1.419(3).

The bonding metrics from the X-ray structure of **1** are consistent with a formal cerium(III)/cerium(III) complex with reduced nitroxide ligands. Two bonding modes of the $[2\text{-}(\text{tBuNO})\text{py}]^-$ anion are observed in **1**. The chelating nitroxide ligands exhibit N–O bond lengths of 1.370(3) and 1.379(3) Å. The bridging nitroxide ligands exhibit a slightly longer N–O

bond length of 1.419(3) Å as a result of the $\mu\text{-}(\text{N},\text{O})$ -bonding mode. For comparison, the reported N–O bond lengths in $\text{La}(\text{hfac})_3(\text{bpybNO})$, where $\text{bpybNO} = 2,2'\text{-bipyridine-}6,6'\text{-diyl bis}(\text{tert-butyl nitroxide})$, with the bpybNO ligand in its neutral, biradical form, are significantly shorter at 1.282(5) and 1.276(6) Å,³⁶ and the N–O bond length in $[(\eta^1\text{-ONC}_5\text{H}_6\text{Me}_4)_2\text{Sm}(\mu\text{-}\eta^1\text{-}\eta^2\text{-ONC}_5\text{H}_6\text{Me}_4)]_2$ is 1.431(8) Å; $[(\eta^1\text{-ONC}_5\text{H}_6\text{Me}_4)_2\text{Sm}(\mu\text{-}\eta^1\text{-}\eta^2\text{-ONC}_5\text{H}_6\text{Me}_4)]_2$ is the product of the reaction of $(\text{C}_5\text{Me}_5)_3\text{Sm}$ with TEMPO (TEMPO = 2,2,6,6-tetramethylpiperidiny-1-oxyl).³⁷ The nitrogen atoms of the tBuNO groups in the chelating nitroxide ligands are planar, as indicated by the sum of the C–N–O, C–N–C, and O–N–C bond angles being $>359.7(3)^\circ$. The $\text{N}_{\text{pyr}}\text{-C-N-O}$ dihedral angles are also $<6^\circ$. These angles indicate that conjugation with the pyridyl ring system is maintained.

The Ce^{III} oxidation state of **1** was confirmed through magnetic susceptibility measurements. The temperature dependence of the magnetic moment for **1** was measured from 2 to 300 K in the presence of a 1.0 T field. The χT value for **1** is 1.46 emu K mol^{-1} at 300 K, which is consistent with the expected values for two isolated $J = 5/2$ Ce^{III} ions.^{38–40} The variable-temperature χT response for **1** is also consistent with reported cerium(III) complexes;^{38–40} the χT product decreases from 1.46 to 1.0 emu K mol^{-1} at 5 K. Below 5 K, the χT product decreases precipitously because of depopulation of the two excited state Kramer's doublets that arise from ligand-field splitting within the $J = 5/2$ manifold of the Ce^{III} ions (Figure S3 in the Supporting Information, SI), although antiferromagnetic coupling between the Ce^{III} moments cannot be ruled out. The field-dependent data at 2 K (Figure S3 in the SI) saturate and achieve a value of 2.17 μB at 7 T. Overall, these data are suggestive of a formal cerium(III)/cerium(III) dimer with fully reduced nitroxide ligands.

The reaction of **1** with 3 equiv of the neutral $2\text{-}(\text{tBuNO})\text{py}$ nitroxide radical in Et_2O immediately formed a dark-purple solution (Scheme 1). Following workup, the homoleptic complex **2** was isolated in 81% yield as a dark-purple powder. Complex **2** is unreactive toward oxygen. Indeed, **2** was synthesized in good yield by the addition of 1 equiv of $2\text{-}(\text{tBuNOH})\text{py}$ to a tetrahydrofuran (THF) suspension of **1** with exposure of the suspension to dry O_2 . The ^1H NMR spectrum of complex **2** showed five sharp peaks in the region of 0–10 ppm, which is expected for a cerium(IV) complex with the four ligands in chemically equivalent environments (Figure S1 in the SI). Slow evaporation of a concentrated THF solution of **2** produced X-ray-quality crystals, allowing for determination of the solid-state structure.

The homoleptic complex **2** crystallizes with the molecule in approximate D_{2d} symmetry (Figure 2). Shape parameters determined for **2** indicate a coordination environment comprising a distorted trigonal dodecahedron (Table 1). The

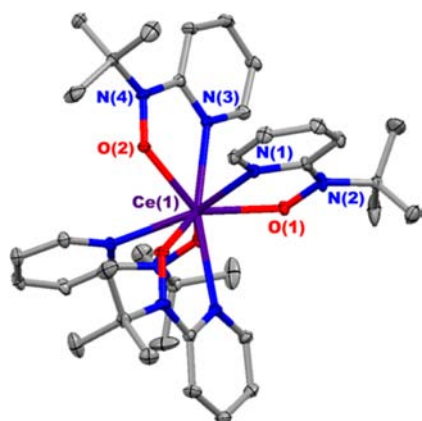


Figure 2. Thermal ellipsoid plot of **2** at 30% probability. Hydrogen atoms are omitted for clarity. Selected bond distances (Å): Ce(1)–N(1) 2.5442(16), Ce(1)–N(3) 2.5383(15), Ce(1)–O(1) 2.2333(13), Ce(1)–O(2) 2.2349(13), N(2)–O(1) 1.377(2), N(4)–O(2) 1.3727(19).

Table 1. Shape Parameters for Complexes **2** and **3**

	ϕ_1	ϕ_2	δ_1	δ_2	δ_3	δ_4	θ_A	θ_B
2	7.8	11.0	30.7	30.9	49.0	49.5	49.4	77.2
3	11.8	15.9	24.2	25.3	48.3	49.2	48.4	78.6
D_{2d}^a	0.0	0.0	29.5	29.5	29.5	29.5	35.2	73.5
D_{4d}^a	24.5	24.5	0.0	0.0	52.4	52.4	57.3	57.3

^aA rigorous D_{2d} geometry corresponds to a regular trigonal dodecahedron, while D_{4d} corresponds to a regular square antiprism.^{41,42}

N–O bond lengths of 1.377(2) and 1.3727(19) Å are similar to those for the chelating ligands in the cerium(III) complex, suggesting that all of the nitroxide ligands are fully reduced. Following the criterion articulated by Parkin,⁴³ the bond distances support the assignment of a formal Ce^{IV} oxidation state in **2**. A decrease in the Ce–O bonds by ~0.13 Å between the chelating nitroxides in **1** and those in **2** is consistent with the smaller ionic radius of the Ce^{IV} ion.⁴⁴ The ^tBuNO groups are also planar about the nitrogen center and coplanar with the pyridine ring.

The Ce^{IV} state of complex **2** was confirmed by Ce L_{III}-edge XAS. Complex **1** showed the single peak characteristic of the Ce^{III} cation, while complex **2** showed the two peaks characteristic of the core hole excitation of the Ce^{IV} ion to final states $2p4f^1\bar{L}5d^1$ and $2p4f^05d^1$, where \bar{L} indicates a ligand hole (Figure 3)⁴⁵

Having established the oxidation state of **2**, we were prompted to examine its reduction chemistry in an effort to isolate a reduced form of the complex. Reduction was possible with the use of potassium mirror, as judged by ¹H NMR spectroscopy, although attempts to crystallize the resulting $K[Ce(2-(^tBuNO)py)_4]$ complex were unsuccessful. However, the exceedingly oxygen-sensitive cerium(III) compound $[K(18-crown-6)(py)_2][Ce(2-(^tBuNO)py)_4]$ (**3**) was ultimately prepared in 57% isolated crystalline yield following the reaction of 1 equiv of $K[2-(^tBuNO)py]$, 3 equiv of 2-(^tBuNOH)py, and 1 equiv of 18-crown-6 with 1 equiv of $Ce[N(SiMe_3)_2]_3$ (Scheme 2). The X-ray structure of **3** revealed N–O and Ce–O distances that were consistent with a cerium(III) complex (Figure 4), as discussed for **1**. The shape parameters for **3** were somewhat changed from those observed for **2** but still largely

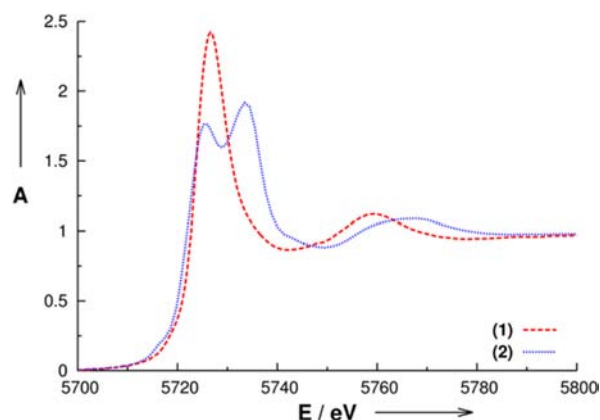


Figure 3. Normalized absorption (A) as a function of the incident X-ray energy (E) in the Ce L_{III}-near-edge region at T = 300 K.

Scheme 2. Synthesis of Complex **3**

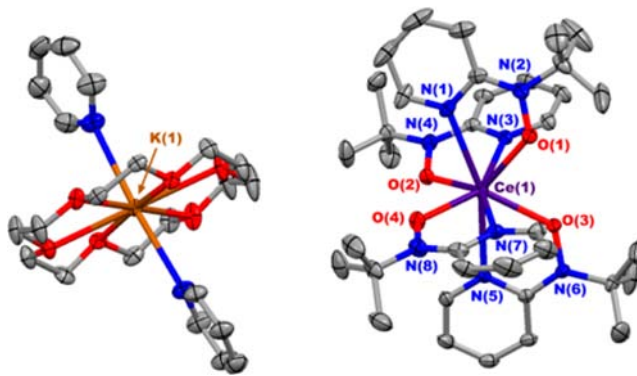
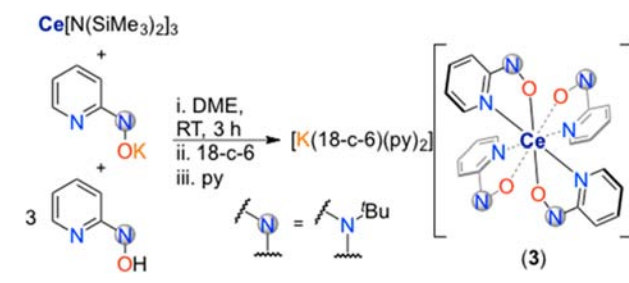


Figure 4. Thermal ellipsoid plot of **3** at 30% probability. Hydrogen atoms are omitted for clarity. Selected bond distances (Å): Ce(1)–N(1) 2.646(3), Ce(1)–N(3) 2.647(3), Ce(1)–N(5) 2.664(3), Ce(1)–N(7) 2.647(3), Ce(1)–O(1) 2.377(3), Ce(1)–O(2) 2.396(2), Ce(1)–O(3) 2.387(2), Ce(1)–O(4) 2.377(3), N(2)–O(1) 1.357(4), N(4)–O(2) 1.372(4), N(6)–O(3) 1.367(4), N(8)–O(4) 1.371(4).

consistent with a distorted trigonal dodecahedral geometry (Table 1).

A variety of oxidants were used to probe the instability of complex **3** in the 3+ oxidation state. Upon the reaction of **3** with ferrocenium hexafluorophosphate, 1,4-benzoquinone, or cobaltocenium triflate, **2** was produced in quantitative yield based on ¹H NMR spectroscopy. Attempts to produce **2** from **3** with decamethylcobaltocenium triflate or benzophenone yielded mixtures of the products, although the reaction with decamethylcobaltocenium triflate clearly produced decamethylcobaltocene through single electron transfer. Together with the observed reduction of **2** using potassium mirror, these oxidation reactions indicated that **3** was a potent reductant

and placed the Ce^{III/IV} redox potential chemically between -1.33 and about -2.00 V versus ferrocene (Fc), which prompted detailed evaluation of the electrochemistry of the system (Table 2).

Table 2. Potentials versus an Internal Ferrocene Standard for Electrochemical Processes in 2-(^tBuNOH)py and 2

	wave 1		wave 2		Ce ^{III/IV}	
	$E_{p,c}$	$E_{p,a}$	$E_{p,c}$	$E_{p,a}$	$E_{p,c}$	$E_{p,a}$
2-(^t BuNOH)py	+0.18	+0.41	-0.38	-0.07	N/A	N/A
2	+0.02	+0.18	-0.58	-0.49	-2.09	-1.80

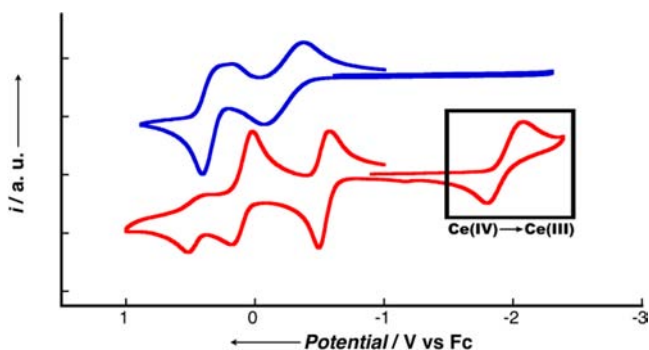


Figure 5. Cyclic voltammograms of complex 2 and 2-(^tBuNOH)py measured in 0.1 M [^mPr₄N][BAR^F₄]/DCM versus an internal Fc standard. The rest potentials were measured at -0.79 V for 2-(^tBuNOH)py and at -0.89 V for 2.

Solution cyclic voltammetry measurements were performed on 2 as well as 2-(^tBuNOH)py in order to evaluate the relative stability of the formal Ce^{IV} oxidation state in complex 2 (Figure 5). The cyclic voltammogram of 2 exhibits four redox couples, with quasi-reversible oxidation waves at $E_{p,a} = -1.80$ V, $E_{p,a} = -0.49$ V, and $E_{p,a} = +0.18$ V versus Fc and an irreversible oxidation wave at $E_{p,a} = +0.52$ V. The cyclic voltammogram of 2-(^tBuNOH)py displayed the corresponding oxidation waves at $E_{p,a} = -0.07$ V and $E_{p,a} = +0.41$ V, indicative of oxidation to the neutral radical and oxoammonium compound, respectively. Given the measured rest potential of -0.89 V, we attribute the features in 2 at $E_{p,a} = -1.80$ V and $E_{p,c} = -2.09$ V to the Ce^{III/IV} redox couple. Solution cyclic voltammetry measurements of complex 3 could not be performed in DCM because the compound slowly oxidized to complex 2 under these conditions. Instead, it was measured in a 20% THF/MeCN mixture. Given a measured rest potential of -1.59 V, the metal-based oxidation feature of 3 was observed at $E_{p,a} = -1.43$ V and $E_{p,c} = -1.68$ V. For comparative purposes, complex 2 was also measured in the 20% THF/MeCN mixture, where the metal-based Ce^{III/IV} redox couple was observed at $E_{p,a} = -1.70$ V and $E_{p,c} = -1.89$ V (Figure S7 in the SI).

Table 3 lists the reduction potentials of several reported cerium(IV) complexes for comparison with 2. Taking a formal half-wave potential for the reduction of 2 at $E_{1/2} = -1.95$ V versus Fc in DCM, it is useful to convert this potential to a saturated calomel electrode (SCE) by adding $+0.46$ V.⁵⁰ The obtained value of -1.49 V versus SCE is shifted by 2.95 versus the standard aqueous potential for the reduction of cerium(IV).⁵¹ However, because of the difference in the dielectric constants between water and acetonitrile, a more effective comparison is that of the reduction potential of [ⁿBu₄N]₂[Ce(NO₃)₆] at $+1.02$ V versus SCE in acetonitrile.⁴⁶ In this

Table 3. Comparison of the Reduction Potential of 2 with Reported Cerium Complexes That Exhibit Reversible or Quasi-Reversible Electrochemical Reduction

complex	$E_{1/2}$ (V vs SCE)	conditions	ref
[ⁿ Bu ₄ N] ₂ [Ce(NO ₃) ₆]	+1.02	MeCN at -40 °C	46
CeCl[N(SiMe ₃) ₂] ₃	+0.26	0.1 M [^m Pr ₄ N][BAR ^F ₄] in DCM	26
Ce(acac) ₄	-0.02	0.1 M TBAPF ₆ in MeCN/acetone	47
Ce(MBP) ₂ (THF) ₂ ^a	-0.37	0.1 M [^m Pr ₄ N][BAR ^F ₄] in THF	27
Ce[(O ₂ C ₆ H ₄) ₄] ⁴⁻	-0.69	5 M NaOH/1 M catechol (aq)	48
Ce(C ₈ H ₈) ₂	-0.8	0.1 M TBAPF ₆ in THF	49
Ce(omtaa) ₂ ^b	-1.1	0.1 M [^m Pr ₄ N][BAR ^F ₄] in THF	25
2	-1.49	0.1 M [^m Pr ₄ N][BAR ^F ₄] in DCM	this work

^aMBP = 2,2'-methylenebis(6-*tert*-butyl-4-methylphenolate). ^bomtaa = 2,3,6,8,11,12,15,17-octamethyldibenzotetraaza[14]annulene.

context, a 2.51 V shift for the cerium(IV) reduction potential in acetonitrile is observed when complexed by four [2-(^tBuNO)py]⁻ ligands. This is greater than the 2.15 V shift observed by Raymond and co-workers for the [Ce(O₂C₆H₄)₄]⁴⁻ anion and represents a 10⁴⁵-fold difference in the formation constants for 2 compared to the anion of 3 in reference to [ⁿBu₄N]₂[Ce(NO₃)₆] in acetonitrile.⁴⁸ The reduction potential for compound 2 is also lower than that reported for cerocene⁴⁹ and for Ce(omtaa)₂, as recently reported by two of us.²⁵

These results indicate that the Ce^{IV} ion is stabilized in the nitroxide ligand framework to an unprecedented degree. This is a noteworthy observation considering that the catecholate ligands of the benchmark complex Ce[(O₂C₆H₄)₄]⁴⁻ comprise two anionic, oxygen-donor sites each that might be expected to more effectively stabilize the Ce^{IV} cation than the [2-(^tBuNO)py]⁻ ligands. In fact, to the best of our knowledge, 2 is the most stable cerium(IV) complex reported on the basis of its quasi-reversible electrochemical reduction potential.⁵³ Following the classification of Connelly and Geiger, complex 3 is best described as a thermodynamically strong reductant, with a reduction potential comparable to that of (C₅Me₅)₂Co, at $E^{\circ} = -1.94$ V vs Fc in DCM.⁵⁰

Support for the strongly stabilized formal Ce^{III/IV} redox couple is also observed in the electronic absorption spectrum of the complex. The UV-vis spectrum of 2 in THF is shown in Figure 6. We attribute the broad band centered at 2.37 eV to a ligand-to-metal charge-transfer transition. The transition at 3.3 eV is assigned to an electronic excitation within the [2-(^tBuNO)py]⁻ ligands, an assignment that was made through comparison with the absorption spectrum of 3 (Figure S8 in the SI). The broadness and intensity of the charge-transfer band at 2.37 eV is suggestive of mixing of vacant Ce 4f and 5d orbitals with filled ligand-based orbitals, a feature that we sought to elucidate with DFT calculations (vide infra).

Electronic Structure Analysis. While lanthanide–ligand bonding has been traditionally viewed as primarily ionic with insignificant 4f orbital contribution,⁵⁴ recent work has explored the possibility for lanthanide complexes to exert stabilization through covalent interactions at the extremes of bonding.^{55–58} In order to determine whether covalent interactions play a role in the stabilization of 2, the electronic structures of the homoleptic cerium nitroxide complexes 2 and 3 were explored

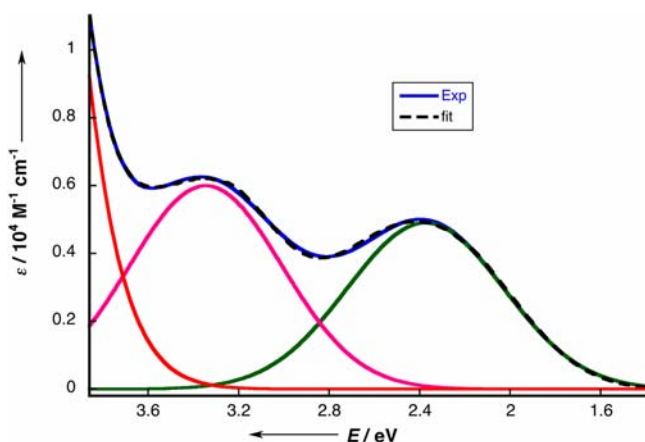


Figure 6. UV-vis electronic absorption spectrum of **2** recorded in THF.⁵² The colored lines are Gaussian fits to the data. The green band is assigned to a LMCT transition and the pink band is assigned to a transition within the $[2-(t\text{BuNO})\text{py}]^-$ ligands.

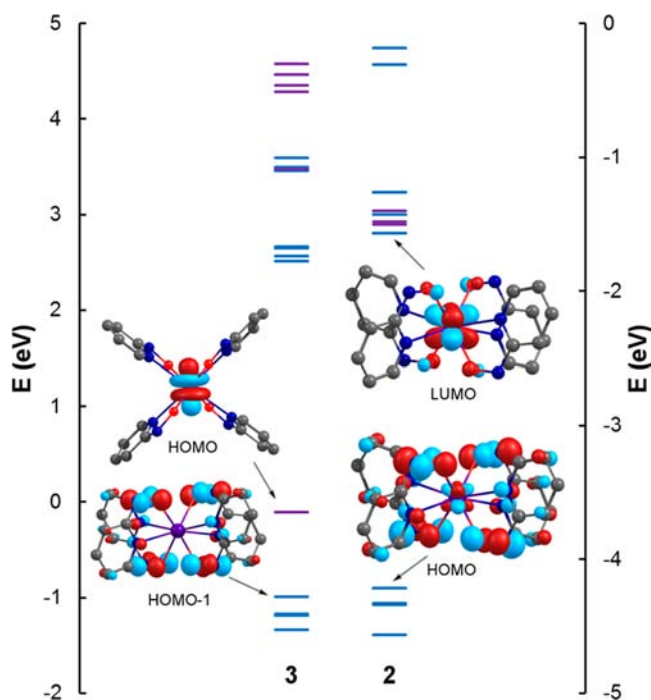


Figure 7. Energy level diagrams for **3** and **2**. The differing energy scales at left and right should be noted. Hydrogen atoms and *tert*-butyl groups are omitted from the inset molecular orbitals for clarity.

using DFT (Figure 7). Both of the calculated structures for the Ce^{IV} and Ce^{III} states accurately predict the Ce–O bond lengths within 0.011 and 0.012 Å, respectively. The calculated Ce– $\text{N}_{(\text{pyr})}$ bond lengths were longer than those experimentally observed but are still within 0.088 and 0.065 Å from the experimentally determined values for **2** and **3**.

In the formal Ce^{IV} state of **2**, the highest occupied molecular orbital (HOMO) has significant electron density located on the $[2-(t\text{BuNO})\text{py}]^-$ ligands with 8.3% Ce 4f character. While there is a tendency for DFT to overemphasize such delocalization, the most striking feature of this orbital is that the N–O bonds of the nitroxide ligands are oriented around the Ce^{IV} ion with the correct symmetry for multiple π -bonding interactions between the four filled N–O π^* orbitals and the $f_z(x^2-y^2)$ atomic

orbital of Ce. In fact, the lowest unoccupied molecular orbital (LUMO) of **2**, calculated to be 2.65 eV above the HOMO, has the correct symmetry for the corresponding π^* interactions. Despite the rather small overlap of the core-like 4f orbitals with ligand-based π^* orbitals, this arrangement possesses the correct symmetry to impose a stabilizing influence on the electronic structure of the complex. A simplified depiction of this orbital interaction is provided in the Figure S9 in the SI. In contrast, in the calculated result of **3**, with Ce in the 3+ oxidation state, the HOMO consists of a single unpaired electron that resides solely in a nonbonding Ce 4f orbital. These results are consistent with the ligand-field analysis of $[\text{Li}(\text{THF})_4][\text{Ce}(\text{COT})_2]$, which showed that the largest single 4f orbital contribution to the single occupied molecular orbital was $4f_z$.⁵⁹

Unlike the Ce^{IV} state in **2**, only minor Ce 4f (<2%) and 5d (<6%) character is observed in other filled orbitals in **3**. The symmetric arrangement of nitroxide π^* orbitals that comprises the HOMO of **2** is present as the HOMO–1 in **3**, without the Ce 4f contribution (Figure 7). The HOMO–1 of **3** was calculated to be 0.88 eV below the HOMO. We propose that oxidation of **3** to **2** lowers the energy of the Ce 4f orbitals, providing a closer energetic matching with the nitroxide N–O π^* orbitals, which leads to greater symmetry-allowed mixing of these metal and ligand orbitals. This effect is further illustrated by fragment molecular orbital analysis, as shown in Figure 7. Figure 7 highlights the isolated $4f_z$ HOMO of **3** and noninteracting 4f and N–O π^* fragments (at left), while the HOMO of **2** includes stabilization from mixing with the $4f_z(x^2-y^2)$ atomic orbital of Ce^{IV} (at right).

The role of ligand-to-metal electron donation in the stabilization of **2** in the 4+ oxidation state was examined through population analysis. A comparison of the natural bond orbital analysis of **2** and **3** with several reported formal cerium(IV) complexes is shown in Table 4. The natural charge

Table 4. Natural Charges (q_{Ce}), Natural Populations (6s, 5d, and 4f), and Mayer Bond Orders (MBOs) of **2** and **3**, Compared to Other Formal Cerium(IV) Complexes

	3 (Ce^{III})	2 (Ce^{IV})	Cp_2CeO (Ce^{IV}) ^a	CeN^*LCl (Ce^{IV}) ^b	$\text{Ce}(\text{COT})_2$ ($\text{Ce}^{\text{III/IV}}$) ^c
q_{Ce}	1.71	1.74	2.42	2.53	2.41
6s	0.16	0.17	0.09	0.16	<i>c</i>
5d	0.92	1.17	0.45	0.36	<i>c</i>
4f	0.14	0.87	1.01	0.95	<i>c</i>
MBO ^d	3.11	4.56			

^aSimilar results were obtained for a series of $\text{Cp}_2\text{Ce}^{\text{IV}}\text{Z}$ ($\text{Z} = \text{F}^+$, O, NH, CH^- , CH_2) compounds.⁶⁰ ^b $\text{N}^* = -\text{N}(\text{SiMe}_3)_2$, $\text{L} = -\text{OCMe}_2\text{CH}_2(\text{CNCH}_2\text{CH}_2\text{NDipp})$, and $\text{Dipp} = 2,6\text{-}i\text{Pr}_2\text{C}_6\text{H}_3$.⁶¹ ^cIndividual populations not reported.⁵⁹ ^dSum of metal–ligand MBOs.

on cerium, q_{Ce} in **2** is essentially unchanged relative to that of **3**, despite the higher formal oxidation state. A smaller natural charge to formal charge ratio is due to greater donation of the nitroxide ligand electron density into unfilled Ce 4f, 5d, and to some extent 6s orbitals, as shown in Table 4. This difference is also reflected in the MBO, which increases dramatically from 3.11 to 4.56 upon oxidation. Notably, the calculated natural charge in **2** is significantly smaller than that in the reported cerium(IV) complexes, indicative of a higher degree of electron donation to the Ce^{IV} cation in this compound. Overall, the DFT-computed results for **2** and **3** and a comparison with reported data suggest a progression of stabilization of the Ce^{IV}

cation that culminates in **2**, consistent with the strong potential needed to reduce the compound.

CONCLUSIONS

We have demonstrated the facile oxidation of a cerium(III) nitroxide complex to a homoleptic cerium(IV) nitroxide complex through the use of a redox-active nitroxide ligand. The resulting complex shows an unprecedented level of stabilization of the 4+ state for cerium. On the basis of the spectroscopic and computational evidence, we attribute stabilization of the 4+ oxidation state in **2** relative to other cerium complexes to the following factors: the hard, ionic interactions between the cerium and oxygen atoms, the symmetry-allowed mixing of the nitroxide π^* orbitals with the Ce^{IV} 4f orbitals provided by the arrangement of nitroxide ligands around the metal center, and the effective energetic matching of the high-energy nitroxide π^* orbitals with the Ce^{IV} 4f orbitals.

The large negative reduction potential required to reduce **2** supports the claim that the geometrical positioning of ligands around cerium can have a dramatic effect on the redox chemistry of the ion, in particular through a δ -bonding combination between the Ce^{IV} cation and ligand field. A similar effect on the stability of the Ce^{IV} oxidation state due to the local site symmetry at cerium has been observed in ceria, CeO_2 , where the cubic site symmetry of the fluorite structure is proposed to be critical for stabilizing the higher oxidation state.¹⁵ In this context, the partially covalent, pseudocubic coordination environment of **2** captures the fundamental bonding interactions found in CeO_2 , in particular the strong thermodynamic preference against reduction for the defect-free material.¹⁵

We expect that appropriate substitution of the pyridyl ring within the $[\text{2}-(t\text{-BuNO})\text{py}]^-$ ligand will enable even further stabilization of the $\text{Ce}^{\text{III/IV}}$ couple; these experiments are underway and their results will be presented in due course.

EXPERIMENTAL SECTION

General Methods. Unless otherwise noted, all reactions and manipulations were performed under an inert atmosphere (N_2) using standard Schlenk techniques or in a Vacuum Atmospheres, Inc., Nexus II drybox equipped with a molecular sieve 13X/Q5 Cu-0226S catalyst purifier system. Glassware was oven-dried for at least 3 h at 150 °C prior to use. ^1H and ^{13}C NMR spectra were obtained on a Bruker DMX-300 Fourier transform NMR spectrometer at 300 and 75.4 MHz, respectively, or a Bruker DRX-500 Fourier transform NMR spectrometer at 500 and 125.6 MHz. Chemical shifts were recorded in units of parts per million downfield of tetramethylsilane, measured by reference to a residual proteo solvent. Elemental analyses were performed at the University of California, Berkeley, Microanalytical Facility using a Perkin-Elmer series II 2400 CHNS analyzer.

Materials. Tetrahydrofuran (THF), dimethoxyethane (DME), diethyl ether (Et_2O), dichloromethane (DCM, CH_2Cl_2), toluene, hexanes, and pentane were purchased from Fisher Scientific. The solvents were sparged for 20 min with dry N_2 and dried using a commercial two-column solvent purification system comprising columns packed with Q5 reactant and neutral alumina, respectively (for hexanes and pentane), or two columns of neutral alumina (for THF, Et_2O , and CH_2Cl_2). Deuterated solvents were purchased from Cambridge Isotope Laboratories, Inc., and stored over potassium mirror overnight prior to use. $\text{Ce}[\text{N}(\text{Si}(\text{CH}_3)_3)_2]_3$ was synthesized as previously described.⁶² The supporting electrolyte, $[\text{Pr}_4\text{N}][\text{B}(3,5\text{-}(\text{CF}_3)_2\text{-C}_6\text{H}_3)_4]$, was prepared according to literature procedures.⁶³

Electrochemistry. Cyclic voltammetry experiments were performed using a CH Instruments 620D Electrochemical Analyzer/

Workstation, and the data were processed using CHI software version 9.24. All experiments were performed in an N_2 atmosphere drybox using electrochemical cells that consisted of a 4 mL vial, a glassy carbon (3-mm-diameter) working electrode, a platinum wire counter electrode, and a silver wire plated with AgCl as a quasi-reference electrode. The working electrode surfaces were polished prior to each set of experiments and periodically replaced on scanning >0 V versus Fc to prevent the buildup of oxidized product on the electrode surfaces. Potentials were reported versus Fc, which was added as an internal standard for calibration at the end of each run. Solutions employed during cyclic voltammetry studies were ~ 3 mM in analyte and 100 mM in $[\text{Pr}_4\text{N}][\text{B}(3,5\text{-}(\text{CF}_3)_2\text{-C}_6\text{H}_3)_4]$ ($[\text{Pr}_4\text{N}][\text{BAr}^{\text{F}}_4]$). All data were collected in a positive-feedback IR compensation mode. The DCM solution cell resistances were measured prior to each run to ensure resistances $\leq \sim 500 \Omega$.⁶³ Scan rate dependences of 50–1000 mV s^{-1} were performed to determine electrochemical reversibility.

Magnetism. Magnetic data were collected using a Quantum Design Multi-Property Measurement System (MPMS-7) with a Reciprocating Sample Option at 2 T from 2 to 300 K and at 2 K from 0 to 7 T. Quartz tubes (3 mm o.d. and 2 mm i.d.), quartz rods, and quartz wool were dried at 250 °C prior to use. The sample tubes were loaded with a finely ground crystalline sample and packed on both sides with quartz wool in the N_2 atmosphere drybox. Quartz wool “slugs” were packed into separate small lengths of quartz “loading tubes” prior to drying to facilitate direct transfer of the slugs into the quartz tube sample holder before and after loading of the sample. The quartz wool slugs were loaded into the sample tube using a quartz “tamping” rod. The sample was loaded through a glass Pasteur pipet that acted as a funnel. The samples and wool were massed to the nearest 0.1 mg with a calibrated and leveled Mettler-Toledo AL-204 analytical balance. Valves with Teflon stopcocks were attached to each end of the tube, and the sample was removed from the glovebox. The samples were flame-sealed under dynamic vacuum on a Schlenk line. A short length of heat-shrink tubing was fitted to one end of the quartz tube and affixed to the tube by treatment with a heat gun. The open end of the heat-shrink tubing was fitted to the end of the MPMS-7 plastic sample transport, without heat shrinking, by fitting a ~ 1 cm length of drinking straw snugly over the tubing/transport assembly. Corrections for the intrinsic diamagnetism of the samples were made using Pascal’s constants.⁶⁴ Data were collected on two independently prepared samples to ensure reproducibility.

X-ray Absorption Spectroscopy. Ce L_{III} -edge XANES data were collected at the Stanford Synchrotron Radiation Lightsources, Beamline 11-2, using a Si 220 ($\varphi = 0$) double monochromator that was detuned to 20% in order to reduce harmonic contamination. The resulting data have an energy resolution of 3.2 eV. Data were collected in transmission, using a CeO_2 reference to calibrate the energy scale, setting the first inflection point of the CeO_2 absorption to 5723 eV. A linear pre-edge background was subtracted, and the data were subsequently normalized at 5800 eV.

Because compound **1** was sensitive to oxygen, each sample was ground into a powder, mixed with dry boron nitride as the diluent, and then packed into the slots of a machined aluminum sample holder. Aluminized mylar was affixed to the holder with an indium-wire seal. After packaging, the samples were transported in dry N_2 -filled containers to the beamline. Sample holders were quickly transferred to the vacuum chamber, exposing the sealed holders to air for less than 30 s before pumping out the chamber and collecting the data under vacuum.

X-ray Crystallography. X-ray intensity data were collected on a Bruker APEXII CCD area detector employing graphite-monochromated Mo K α radiation ($\lambda = 0.71073 \text{ \AA}$) at a temperature of 143(1) K. In all cases, rotation frames were integrated using S AINT ,⁶⁵ producing a listing of unaveraged F^2 and $\sigma(F^2)$ values that were then passed to the SHELXTL⁶⁶ program package for further processing and structure solution on a Dell Pentium 4 computer. The intensity data were corrected for Lorentz and polarization effects and for absorption using TWINABS⁶⁷ or SADABS.⁶⁸ The structures were solved by direct methods (SHELXS-97).⁶⁹ Refinement was by full-matrix least squares based on F^2 using SHELXL-97.⁶⁹ All reflections were used during

refinements. Non-hydrogen atoms were refined anisotropically, and hydrogen atoms were refined using a riding model.

Synthesis of $[\text{Ce}^{\text{III}}(\mu\text{-}^t\text{BuNOpy})(2\text{-}^t\text{BuNOpy})_2]_2$ (1). White solid *N*-^tBu-*N*-2-pyridylhydroxylamine³⁵ (0.24 g, 1.44 mmol, 3 equiv) was dissolved in 5 mL of Et₂O in a 20 mL scintillation vial to produce a clear, colorless solution. A clear, yellow pentane solution (10 mL) of Ce[N(SiMe₃)₂]₃ (0.30 g, 0.48 mmol, 1 equiv) was layered upon the ether solution. The vial was set undisturbed at room temperature overnight, and X-ray-quality red-orange crystals formed from the mixture. The crystals were isolated by vacuum filtration, rinsed with Et₂O and pentane, and dried under reduced pressure, yielding **1** (0.20 g, 0.16 mmol, 67% crystalline yield). Anal. Calcd for C₅₄H₇₈O₆N₁₂Ce₂: C, 51.01; H, 6.18; N, 13.22. Found: C, 51.02; H, 6.25; N, 13.05.

Synthesis of $\text{Ce}[2\text{-}^t\text{BuNOpy}]_4$ (2). White solid *N*-^tBu-*N*-2-pyridylhydroxylamine (0.12 g, 0.72 mmol, 3 equiv) was dissolved in 15 mL of Et₂O, and solid PbO₂ (1.02 g, 4.33 mmol, 18 equiv) was added. The suspension was stirred for 2 h to produce a red-orange solution. The mixture was filtered through a Celite-packed coarse-porosity fritted filter into a 125 mL filter flask charged with Ce^{III}(μ-^tBuNOpy)(2-^tBuNOpy)₂ (0.30 g, 0.24 mmol, 1 equiv) suspended in 40 mL of Et₂O. Upon addition, **1** immediately dissolved and a dark-purple solution formed. The reaction was stirred for 14 h, after which Et₂O was removed under reduced pressure to produce a dark powder. The powder was washed with pentane until the washings were colorless, and the dark-purple **2** was dried under reduced pressure (0.311 g, 0.39 mmol, 81% yield). X-ray-quality crystals were obtained from slow evaporation of a nearly saturated THF solution of the complex. Anal. Calcd for C₃₆H₅₂O₄N₈Ce: C, 53.98; H, 6.54; N, 13.99. Found: C, 53.92; H, 6.64; N, 13.88. ¹H NMR (300 MHz, C₆D₆): δ 9.05 (ddd, *J* = 5.6, 2.0, and 1.0 Hz, 1H, *Ar-H*), 6.75 (ddd, *J* = 8.9, 6.6, and 2.0 Hz, 1H, *Ar-H*), 6.44 (dd, *J* = 8.9 and 1.0 Hz, 1H, *Ar-H*), 6.20 (ddd, *J* = 6.6, 5.6, and 1.0 Hz, 1H, *Ar-H*), 1.30 (s, 9H, C(CH₃)₃). ¹³C NMR (125.6 MHz, C₆D₆): δ 159.2 (*Ar-C*), 148.9 (*Ar-C*), 135.0 (*Ar-C*), 110.4 (*Ar-C*), 108.9 (*Ar-C*), 61.7 (C(CH₃)₃), 29.0 (C(CH₃)₃).

Synthesis of $[\text{K}(18\text{-crown-6})(\text{pyr})_2][\text{Ce}(2\text{-}^t\text{BuNOpy})_4]$ (3). Potassium *N*-^tBu-*N*-2-pyridylhydroxylamine was synthesized by the addition of K[N(SiMe₃)₂] (0.32 g, 1.6 mmol, 0.9 equiv) to an Et₂O solution of *N*-^tBu-*N*-2-pyridylhydroxylamine (0.30 g, 1.8 mmol, 1 equiv). Yellow solid crashed out immediately, but stirring was continued for 2 h to ensure complete conversion. The solid was washed with Et₂O and dried under reduced pressure to afford potassium *N*-^tBu-*N*-2-pyridylhydroxylamine in 93% yield.

To a mixture of *N*-^tBu-*N*-2-pyridylhydroxylamine (0.040 g, 0.24 mmol, 3 equiv) and potassium *N*-^tBu-*N*-2-pyridylhydroxylamine (0.017 g, 0.080 mmol, 1 equiv) dissolved in DME (5 mL) was added a DME (2 mL) solution of Ce[N(SiMe₃)₂]₃ (0.050 g, 0.080 mmol, 1 equiv). The reaction immediately turned dark red. Volatiles were removed in vacuo after 3 h, leaving an orange powder. The addition of 1 equiv of 18-crown-6 was made to this orange powder, and the mixture was dissolved in 1 mL of pyridine. Layering pentane (~4 mL) at -25 °C resulted in the formation of complex **3** as X-ray-quality block red crystals in 57% yield. Anal. Calcd for C₅₈H₈₆KN₁₀O₁₀Ce: C, 55.17; H, 6.87; N, 11.09. Found: C, 55.21; H, 6.88; N, 11.06.

Oxidation Reactions of 3. To a 20 mL scintillation vial equipped with a magnetic stir bar were dissolved in THF (2 mL) 1 equiv of complex **3** (0.020 g, 0.016 mmol, 1 equiv) and 1 equiv of oxidant (FcPF₆, 1,4-benzoquinone, or [CoCp₂]OTf). The reaction immediately turned purple and was allowed to react for 2 h. THF was removed under reduced pressure, and the products were dissolved in C₆D₆. The reactions were analyzed by ¹H NMR spectroscopy.

To a 20 mL scintillation vial equipped with a magnetic stir bar were dissolved in THF (2 mL) 1 equiv of complex **3** (0.020 g, 0.016 mmol, 1 equiv) and 1 equiv of benzophenone (0.003 g, 0.016 mmol). No immediate color change to purple was observed. The reaction was allowed to react for 2 h. THF was removed under reduced pressure, and the products were dissolved in C₆D₆. The reaction was analyzed by ¹H NMR spectroscopy.

To a 20 mL scintillation vial equipped with a magnetic stir bar were dissolved in THF (2 mL) 1 equiv of complex **3** (0.020 g, 0.016 mmol,

1 equiv). [CoCp₂]OTf (0.008 g, 0.016 mmol, 1 equiv) was dissolved in MeCN (2 mL) and added to the reaction mixture. No immediate color change to purple was observed. The reaction was allowed to react for 2 h. THF was removed under reduced pressure, and the products were dissolved in C₆D₆. The reaction was analyzed by ¹H NMR spectroscopy.

■ ASSOCIATED CONTENT

Supporting Information

X-ray crystallographic files (CIFs), ¹H and ¹³C NMR data, magnetism data, and electrochemical data. This material is available free of charge via the Internet at <http://pubs.acs.org>.

■ AUTHOR INFORMATION

Corresponding Author

*E-mail: schelter@sas.upenn.edu.

Notes

The authors declare no competing financial interest.

■ ACKNOWLEDGMENTS

E.J.S. acknowledges the U.S. Department of Energy, Office of Science, Early Career Research Program (Grant DE-SC0006518), and the University of Pennsylvania for financial support of this work. We thank Prof. Raymond J. Gorte, University of Pennsylvania, for helpful discussion. This work used the Extreme Science and Engineering Discovery Environment (XSEDE), which is supported by National Science Foundation Grant OCI-1053575. Portions of this work were supported by the Director, Office of Science (OS), Office of Basic Energy Sciences, of the U.S. Department of Energy (DOE) under Contract DE-AC02-05CH11231 and were carried out at SSRL, a Directorate of SLAC National Accelerator Laboratory and an OS User Facility operated for the DOE OS by Stanford University.

■ REFERENCES

- (1) Pierre, D.; Deng, W.; Flytzani-Stephanopoulos, M. *Top. Catal.* **2007**, *46*, 363–373.
- (2) Fu, Q.; Saltsburg, H.; Flytzani-Stephanopoulos, M. *Science* **2003**, *301*, 935–938.
- (3) Wang, Q.; Zhao, B.; Li, G.; Zhou, R. *Environ. Sci. Technol.* **2010**, *44*, 3870–3875.
- (4) Matsumoto, S. *Ä. Catal. Today* **2004**, *90*, 183–190.
- (5) Kharton, V. V.; Figueiredo, F. M.; Navarro, L.; Naumovich, E. N.; Kovalevsky, A. V.; Yaremchenko, A. A.; Viskup, A. P.; Carneiro, A.; Marques, F. M. B.; Frade, J. R. *J. Mater. Sci.* **2001**, *36*, 1105–1117.
- (6) Lu, C.; Worrell, W. L.; Wang, C.; Park, S.; Kim, H.; Vohs, J. M.; Gorte, R. J. *Solid State Ionics* **2002**, *152–153*, 393–397.
- (7) Wang, D.; Kang, Y.; Doan-Nguyen, V.; Chen, J.; Küngas, R.; Wieder, N. L.; Bakhmutsky, K.; Gorte, R. J.; Murray, C. B. *Angew. Chem., Int. Ed.* **2011**, *50*, 4378–4381.
- (8) Kim, C. K.; Kim, T.; Choi, I.-Y.; Soh, M.; Kim, D.; Kim, Y.-J.; Jang, H.; Yang, H.-S.; Kim, J. Y.; Park, H.-K.; Park, S. P.; Park, S.; Yu, T.; Yoon, B.-W.; Lee, S.-H.; Hyeon, T. *Angew. Chem., Int. Ed.* **2012**, *51*, 11039–11043.
- (9) Li, M.; Shi, P.; Xu, C.; Ren, J.; Qu, X. *Chem. Sci.* **2013**, *4*, 2536–2542.
- (10) Wason, M. S.; Zhao, J. *Am. J. Transl. Res.* **2013**, *5*, 126–131.
- (11) Paier, J.; Penschke, C.; Sauer, J. *Chem. Rev.* **2013**, *113*, 3949–3985.
- (12) Wang, H.-F.; Li, H.-Y.; Gong, X.-Q.; Guo, Y.-L.; Lu, G.-Z.; Hu, P. *Phys. Chem. Chem. Phys.* **2012**, *14*, 16521–16535.
- (13) Skorodumova, N. V.; Simak, S. I.; Lundqvist, B. I.; Abrikosov, I. A.; Johansson, B. *Phys. Rev. Lett.* **2002**, *89*, 166601.
- (14) Trovarelli, A. *Catal. Sci. Ser.* **2002**, *2*, 15–50.

- (15) Gorte, R. J. *AIChE J.* **2010**, *56*, 1126–1135.
- (16) Stubenrauch, J.; Vohs, J. M. *J. Catal.* **1996**, *159*, 50–57.
- (17) Cordatos, H.; Bunluesin, T.; Stubenrauch, J.; Vohs, J. M.; Gorte, R. J. *J. Phys. Chem.* **1996**, *100*, 785–789.
- (18) Riedel, S.; Kaupp, M. *Coord. Chem. Rev.* **2009**, *253*, 606–624.
- (19) Wang, X.; Andrews, L.; Riedel, S.; Kaupp, M. *Angew. Chem., Int. Ed.* **2007**, *46*, 8371–8375.
- (20) Gross, Z.; Gray, H. B. *Comments Inorg. Chem.* **2006**, *27*, 61–72.
- (21) Scepianiak, J. J.; Vogel, C. S.; Khusniyarov, M. M.; Heinemann, F. W.; Meyer, K.; Smith, J. M. *Science* **2011**, *331*, 1049–1052.
- (22) Vogel, C.; Heinemann, F. W.; Sutter, J.; Anthon, C.; Meyer, K. *Angew. Chem., Int. Ed.* **2008**, *47*, 2681–2684.
- (23) Kropp, H.; King, A. E.; Khusniyarov, M. M.; Heinemann, F. W.; Lancaster, K. M.; DeBeer, S.; Bill, E.; Meyer, K. *J. Am. Chem. Soc.* **2012**, *134*, 15538–15544.
- (24) Robinson, J. R.; Booth, C. H.; Carroll, P. J.; Walsh, P. J.; Schelter, E. J. *Chem.—Eur. J.* **2013**, *19*, 5996–6004.
- (25) Williams, U. J.; Mahoney, B. D.; Lewis, A. J.; DeGregorio, P. T.; Carroll, P. J.; Schelter, E. J. *Inorg. Chem.* **2013**, *52*, 4142–4144.
- (26) Robinson, J. R.; Carroll, P. J.; Walsh, P. J.; Schelter, E. J. *Angew. Chem., Int. Ed.* **2012**, *51*, 10159–10163.
- (27) Mahoney, B. D.; Piro, N. A.; Carroll, P. J.; Schelter, E. J. *Inorg. Chem.* **2013**, *52*, 5970–5977.
- (28) Eller, P. G.; Penneman, R. A. *J. Less-Common Met.* **1987**, *127*, 19–33.
- (29) Hobart, D. E.; Samhoun, K.; Young, J. P.; Norvell, V. E.; Mamantov, G.; Peterson, J. R. *Inorg. Nucl. Chem. Lett.* **1980**, *16*, 321–328.
- (30) Payne, G. F.; Peterson, J. R. *J. Less-Common Met.* **1986**, *126*, 371–377.
- (31) Amiel-Levy, M.; Hoz, S. *J. Am. Chem. Soc.* **2009**, *131*, 8280–8284.
- (32) Choquette, K. A.; Sadasivam, D. V.; Flowers, R. A. *J. Am. Chem. Soc.* **2010**, *132*, 17396–17398.
- (33) Labouille, S. p.; Nief, F. o.; Le Goff, X.-F. d. r.; Maron, L.; Kindra, D. R.; Houghton, H. L.; Ziller, J. W.; Evans, W. J. *Organometallics* **2012**, *31*, 5196–5203.
- (34) Molander, G. A. *Chem. Rev.* **1992**, *92*, 29–68.
- (35) Bogart, J. A.; Lee, H. B.; Boreen, M. A.; Jun, M.; Schelter, E. J. *J. Org. Chem.* **2013**, *78*, 6344–6349.
- (36) Koide, K.; Ishida, T. *Inorg. Chem. Commun.* **2011**, *14*, 194–196.
- (37) Evans, W. J.; Perotti, J. M.; Doedens, R. J.; Ziller, J. W. *Chem. Commun.* **2001**, 2326–2327.
- (38) Evans, W. J.; Hozbor, M. A. *J. Organomet. Chem.* **1987**, *326*, 299–306.
- (39) Stults, S. D.; Andersen, R. A.; Zalkin, A. *Organometallics* **1990**, *9*, 115–122.
- (40) Walter, M. D.; Fandos, R.; Andersen, R. A. *New J. Chem.* **2006**, *30*, 1065–1070.
- (41) Muetterties, E. L.; Guggenberger, L. J. *J. Am. Chem. Soc.* **1974**, *96*, 1748–1756.
- (42) Hoard, J. L.; Silverton, J. V. *Inorg. Chem.* **1963**, *2*, 235–242.
- (43) Parkin, G. J. *Chem. Educ.* **2006**, *83*, 791.
- (44) Shannon, R. *Acta Crystallogr., Sect. A* **1976**, *32*, 751–767.
- (45) Booth, C. H.; Walter, M. D.; Daniel, M.; Lukens, W. W.; Andersen, R. A. *Phys. Rev. Lett.* **2005**, *95*, 267202.
- (46) Zheng, H.; Yoo, S. J.; Münck, E.; Que, L. *J. Am. Chem. Soc.* **2000**, *122*, 3789–3790.
- (47) Behrsing, T.; Bond, A. M.; Deacon, G. B.; Forsyth, C. M.; Forsyth, M.; Kamble, K. J.; Skelton, B. W.; White, A. H. *Inorg. Chim. Acta* **2003**, *352*, 229–237.
- (48) Sofen, S. R.; Cooper, S. R.; Raymond, K. N. *Inorg. Chem.* **1979**, *18*, 1611–1616.
- (49) Streitwieser, A.; Kinsley, S. A.; Jenson, C. H.; Rigsbee, J. T. *Organometallics* **2004**, *23*, 5169–5175.
- (50) Connelly, N. G.; Geiger, W. E. *Chem. Rev.* **1996**, *96*, 877–910.
- (51) Smith, G. F.; Getz, C. A. *Ind. Eng. Chem. Anal. Ed.* **1938**, *10*, 191–195.
- (52) The fityk software, Wojdyr, M. *J. Appl. Cryst.* **2010**, *43*, 1126–1128, was used to fit the data to three Gaussian curves.
- (53) A cerium complex with a comparable shift in the Ce^{III/IV} redox potential has been recently reported. However, the wave is extremely irreversible ($E_{pa} = -1.70$ V; $E_{pc} = -2.39$ V), and it seems that new chemical species may be forming upon electrochemical reduction. See: Broderick, E. M.; et al. *Inorg. Chem.* **2011**, *50*, 2870–2877.
- (54) Maron, L.; Eisenstein, O. *J. Phys. Chem. A* **2000**, *104*, 7140–7143.
- (55) Saleh, L. M. A.; Birjkumar, K. H.; Protchenko, A. V.; Schwarz, A. D.; Aldridge, S.; Jones, C.; Kaltsoyannis, N.; Mountford, P. *J. Am. Chem. Soc.* **2011**, *133*, 3836–3839.
- (56) Minasian, S. G.; Krinsky, J. L.; Arnold, J. *Chem.—Eur. J.* **2011**, *17*, 12234–12245.
- (57) Krinsky, J. L.; Minasian, S. G.; Arnold, J. *Inorg. Chem.* **2011**, *50*, 345–357.
- (58) Denning, R. G.; Harmer, J.; Green, J. C.; Irwin, M. *J. Am. Chem. Soc.* **2011**, *133*, 20644–20660.
- (59) Ferraro, F.; Barboza, C. A.; Arratia-Pérez, R. *J. Phys. Chem. A* **2012**, *116*, 4170–4175.
- (60) Clark, D. L.; Gordon, J. C.; Hay, P. J.; Poli, R. *Organometallics* **2005**, *24*, 5747–5758.
- (61) Arnold, P. L.; Turner, Z. R.; Kaltsoyannis, N.; Pelekanaki, P.; Bellabarba, R. M.; Tooze, R. P. *Chem.—Eur. J.* **2010**, *16*, 9623–9629.
- (62) Bradley, D. C.; Ghotra, J. S.; Hart, F. A. *J. Chem. Soc., Dalton Trans.* **1973**, 1021–1023.
- (63) Thomson, R. K.; Scott, B. L.; Morris, D. E.; Kiplinger, J. L. *C. R. Chimie* **2010**, *13*, 790–802.
- (64) Bain, G. A.; Berry, J. F. *J. Chem. Educ.* **2008**, *85*, 532.
- (65) SAINT; Bruker AXS Inc.: Madison, WI, 2009.
- (66) SHELXTL; Bruker AXS Inc.: Madison, WI, 2009.
- (67) Sheldrick, G. M. TWINABS; University of Göttingen: Göttingen, Germany, 2008.
- (68) Sheldrick, G. M. SADABS; University of Göttingen: Göttingen, Germany, 2007.
- (69) Sheldrick, G. *Acta Crystallogr., Sect. A* **2008**, *64*, 112–122.